DOI: 10.1002/cmdc.200800217

Discovery of Novel Anticancer Compounds Based on a Quinoxalinehydrazine Pharmacophore

Jinxia Deng,[a] Laleh Taheri,[a] Fedora Grande,[a, b] Francesca Aiello,[a, b] Antonio Garofalo,[b] and Nouri Neamati*[a]

*Quinoxalinehydrazines represent a novel class of compounds with excellent potency in a panel of cancer cell lines. A prototype compound, SC144, showed significant in vivo efficacy in mice xenograft models of human breast cancer cells. The subsequent structure–activity relationship study resulted in the discovery of SC161 with better potency in cancer cell lines. Further exploring the possible conformational space by a 10 ns molecular dynamics simulation as presented herein, resulted in various pharmacophore orientations. The trajectory analysis indicated that in most of the simulation time, the molecule stays favorably in a compact planarlike orientation. We therefore built a pharmacophore model based on the cluster containing the highest number of frames to represent the most probable orientation. The model was used to screen a subset of our small molecule database containing 350,000 compounds. We selected 35 compounds for the initial cytotoxicity screen. Seventeen compounds belonging to oxadiazolopyrazine and quinoline class displayed cytotoxicity in various cancer cell lines. Five of them, compounds **2**, **6**, **15, 16**, and **19**, all bearing an oxadiazolopyrazine scaffold, showed IC_{50} values <3 μM in certain tumor cell lines. The most potent compound, **2**, showed IC_{50} values <2 μM in HCT116 $p53^{+/+}$, HCT116 $p53^{-/-}$, and HEY cells, and 8 μM in NIH3T3 cells. This study shows that conformational sampling of a lead small molecule followed by representative pharmacophore model development is an efficient approach for the rational design of novel anticancer agents with similar or better potency than the original lead but with different physicochemical properties.*

Introduction

With the recent advances in targeted therapeutics and the progress in new approaches in target identification, novel anticancer agents with new mechanisms of action are under intensive investigation. We have previously shown that the class of salicylhydrazide compounds (SC) exhibited nanomolar range potency in a panel of human cancer cell lines. In as yet unpublished data, we have discovered that SC144, a prototype of a series of quinoxalinehydrazines, demonstrated significant in vivo efficacy in mice xenograft models of human breast cancer cells. Recently, we reported structure–activity relationship studies by preparing a series of compounds using a one-step coupling of 4-chloropyrrolo[1,2-*a*]quinoxalines with pyrazin-2-carbohydrazide. The newly synthesized compounds were tested against four human cancer cell lines by both MTT and colony formation assays. These assays revealed that the substitution at the 2-carbohydrazide moiety had a profound effect on the activity of the drugs, and that SC161 showed much higher activity than other analogues.[1] While the specific target and mechanism of SC161 is currently under investigation in our laboratory, herein, we have further explored SC161 as a lead molecule to design anticancer agents with better potency and different pharmacokinetic properties.

The pharmacophore concept has been widely accepted as an efficient tool for use in combination with various other technologies in drug design and optimization.[2–6] In general, pharmacophore models can be generated either using a set of known inhibitors or the active site of the enzyme. Ligand-based pharmacophore models are generated by utilizing a set of known inhibitors. The use of pharmacophore models as search queries are expected to retrieve novel compounds that contain desirable pharmacophore features with diverse structural and chemical features. These compounds are then expected to bind to the drug target in a similar manner as the model compounds and to exert a similar biological response. This provides an extensive chemical space for lead identification and optimization. Receptor-based pharmacophore models are generated based on key chemical features in the active site of an enzyme. The use of models as search queries is expected to retrieve compounds containing complementary pharmacophoric features and shape. A receptor-based approach requires detailed and accurate information on the key features of the enzyme active site that are involved in drug binding.[7] Both pharmacophore model approaches have been successfully reported in identifying novel inhibitors specific to certain drug targets (for examples, see references [8–10]).

In this study, we focused on potent lead compound SC161 and carried out a 10 ns molecular dynamics (MD) simulation

[a] *J. Deng, L. Taheri, F. Grande, F. Aiello, N. Neamati*
Department of Pharmacology and Pharmaceutical Sciences
School of Pharmacy, University of Southern California, 1985 Zonal Avenue
Los Angeles, California 90089 (USA)
Fax: (+1) 323-442-1390
E-mail: neamati@usc.edu

[b] *F. Grande, F. Aiello, A. Garofalo*
Dipartimento di Scienze Farmaceutiche
Università della Calabria, 87036 Arcavacata di Rende (Cs) (Italy)

followed by cluster analysis of the trajectories. Then, a 3D pharmacophore model was accordingly developed on the basis of the representative conformation from a selected cluster to capture the high probabilistic feature orientation. Next, the pharmacophore model was applied to screen a subset of our small molecule database. Finally, we selected novel compounds and tested them against a panel of cancer cell lines to confirm their cytotoxicity.

Results and Discussions

MD trajectory and cluster analysis

We previously applied MD simulations on HIV-1 integrase to develop dynamic pharmacophore models bearing features complementary to the target. The models were used as searching queries to screen small molecule databases and identified novel integrase inhibitors.[8,11,12] In this study however, we employed a similar technique with a small-molecule lead, SC161. The MD simulation was carried out in explicit water environment at the NVT ensemble. Energy profile over each 10 ns showed that the whole system had an average potential energy of $-16576.1\ kJ\,mol^{-1}$ with $<0.6\%$ fluctuation, and an average kinetic energy of 3189 $kJ\,mol^{-1}$ with $<2.0\%$ fluctuation. The total energy of the whole equilibrated system was $-13386\ kJ\,mol^{-1}$ with 0.6% fluctuation, indicating the system was in its well-established stable state. The average simulation temperature was at 300 K with fluctuation less than 6 K.

Defined variables for measuring the conformational change

To characterize the conformational changes, six parameters were initially defined to analyze the dynamic behavior of SC161. As shown in Figure 1, two variables, *d1* and *d2*, were defined to sample the distance fluctuation between atom pairs of N24 and O18, and of O18 and N13 (Figure 1b), respectively. In addition, three torsional angles were monitored during the simulations. Those were *t1* defined by atoms N13-C14-N15-N16, *t2* defined by C14-N15-N16-C17, and *t3* defined by atoms N16-C17-C19-C20. In addition, a planar angle was defined describing the orientation between the planes set by the two aromatic fragments of SC161. Plane I (P1 hereafter) was defined by three atoms, C19, N21, and N24 of the pyrazine motif, and plane II (P2 hereafter) was defined by N5, N13, and C14 of the quinoxaline scaffold.

Correlations among defined variables

Apparently, the conformational behavior was strictly dependent on the three flexible dihedral angles, which could consistently be monitored by the planar angle defined above and the two distances *d1* and *d2*. Figures 2 and 3 describe the dynamic behavior of SC161 by means of the time-dependence of the defined variables. The snapshots were recorded at intervals of 2 ps, and a total of 5001 frames represented the 10 ns simulation studies. Among the three torsional angles, *t1* (Figure 2a, blue) is highly populated at a value close to 0° or 360°, which

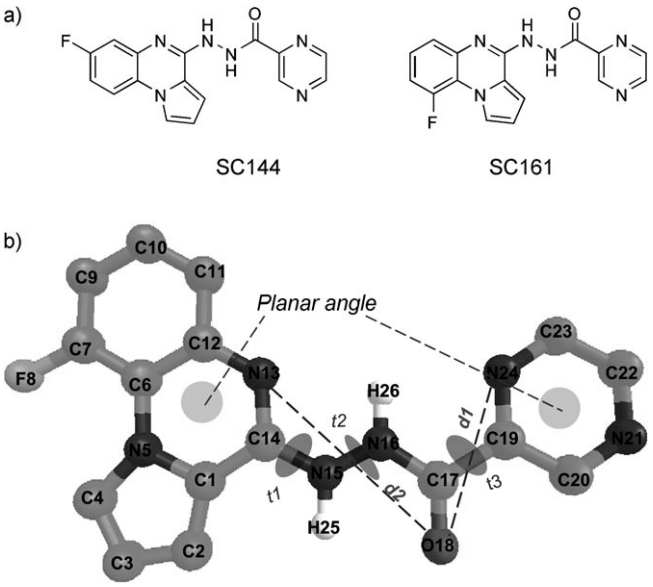

Figure 1. Structures of SC144 and SC161 and parameters defined to monitor the conformational behavior of SC161. Defined variables: *d1*: O18-N24; *d2*: O18-N13; flexible torsion angles: *t1*:N13-C14-N15-N16, *t2*:C14-N15-N16-C17, *t3*: N16-C17-C19-C20; Planar angle is defined by two planes as represented by two gray surfaces: P1-C19N21N24 and P2-N5N13C14.

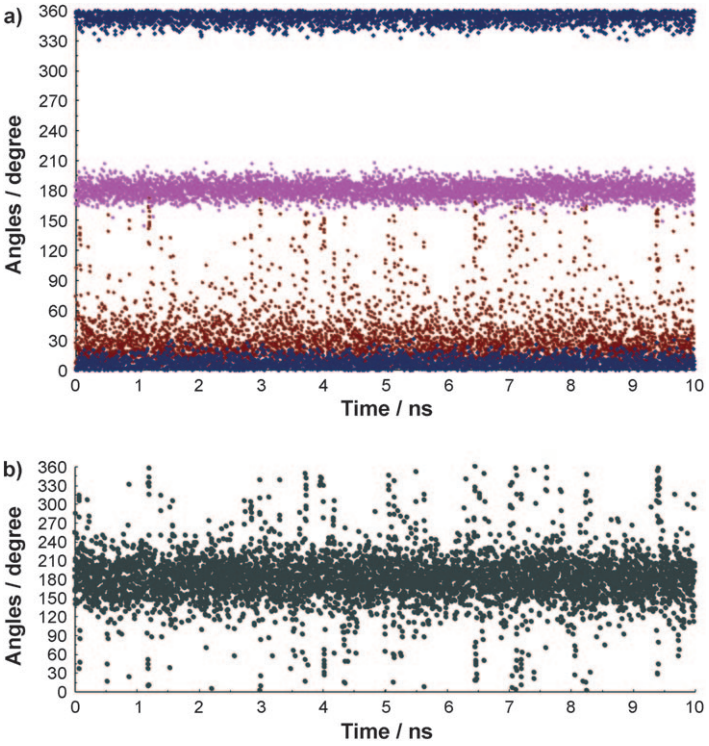

Figure 2. Time dependence of the three flexible torsional angles and the planar angle behavior during the simulation. a) *t1*: blue; *t2*: pink; *t3*: green; b) planar angle: gray.

represents the same orientation of the molecule, whereas *t2* (pink in Figure 2a) stabilizes at its average of 180° with very small fluctuation. This indicates that the two torsion angles, *t1*

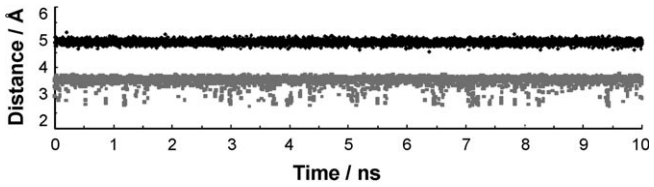

Figure 3. Time dependence of the two distance variables during the simulation, *d1*: gray and *d2*: black.

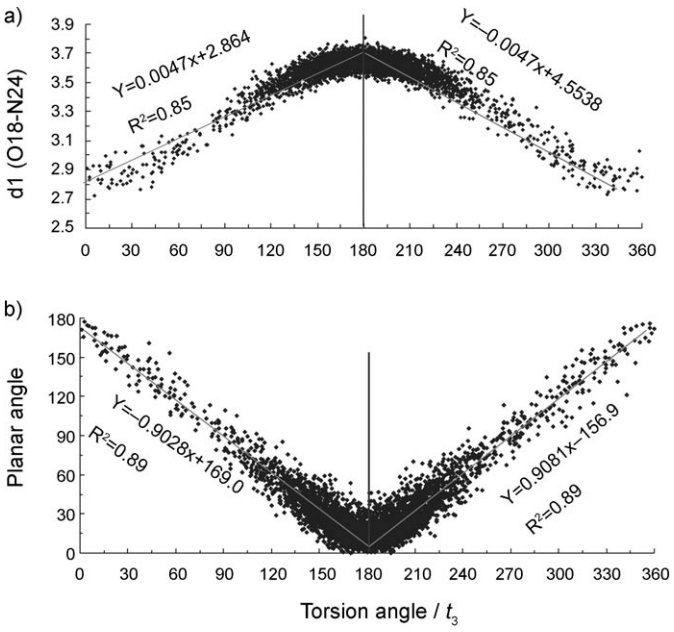

Figure 4. Regression analysis shows linear relationship between distance *d1* (O18-N24) and the torsion angle *t3* (N13-C14-N15-N16), and strong correlation between planar angle and the torsion angle *t3*.

and *t2*, are rather stable, and that no major conformational change occurred to the quinoxalinehydrazine motif of SC161, which is consistently depicted by the *d2* (Figure 3, black) index averaged at 4.8 Å. This observation indicates that *t1*, *t2*, and *d2* are not critical for conformational analysis and therefore are not considered further. However, torsion angle, *t3* (Figure 2b, gray), apparently samples a larger angle space by covering an entire range of 0–360°. This consequently leads to the wide range fluctuation of both planar angle (red in Figure 2a) ranging from 0–180°, and the *d1* (Figure 3, gray) value ranging from 2.7 Å (*cis* position) to 3.8 Å (*trans* position) around its average of 3.5 Å. As a result, the hydrazine motif actively flips at different angles leading to the various conformational clusters of SC161.

Furthermore, we performed regression analysis to better understand the correlation of torsion angle *t3*, distance *d1*, and the planar angle. Figure 4a shows a nearly symmetric profile of distance *d1* versus torsion angle *t3* with respect to the *t3* value of 180°, and a strong correlation between *d1* and *t3* with the correlation coefficient of 0.92 ($R^2 = 0.85$). Likewise, planar angle was selected and further correlated with the torsion angle, *t3*, as described by the scatter plot in Figure 4b. This shows a strong linear correlation between the two variables as well aligned by the linear equation functions (symmetric with respect to the *t3* value of 180) and with a correlation coefficient of 0.95 ($R^2 = 0.89$, respectively). The regression analysis therefore confirms that the conformational change of SC161 solely depends on the behavior of torsion *t3*.

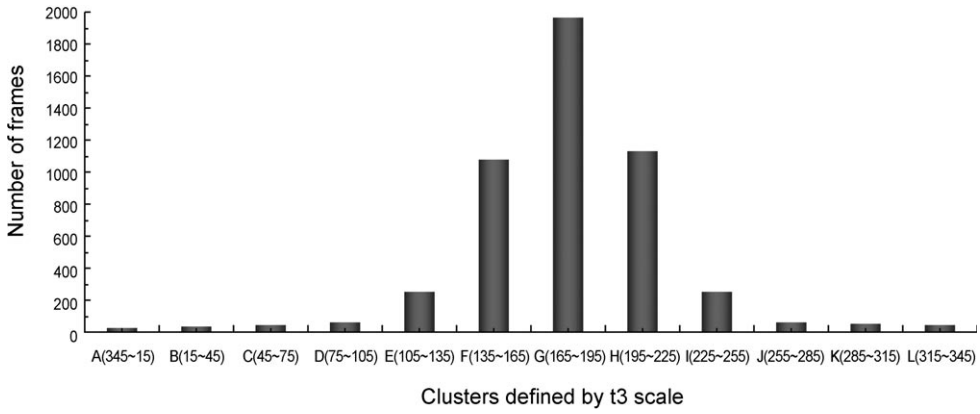

Figure 5. Population of clusters grouped by the value range of torsion angle, *t3*. Each cluster covers the conformations with *t3* values ranging within 30°. For example cluster B has frames with *t3* ranging from 15–45° and cluster C with *t3* values from 45–75°, and so on, except cluster A with *t3* values in the range of 345–15°.

Snapshots cluster analysis

As discussed above, we clustered the conformation of SC161 simply based on the distributions of *t3* value, which were calculated from 5001 snapshots. Figure 5 shows the population profile of the twelve clusters with an incremental step of 30° in *t3* value. As a result of the overlap between the conformations at *t3* values of 0° and 360°, the first cluster contained the frames with *t3* ranging from 0–15° and 345–360°, labeled as cluster A (345–15°). Subsequently, cluster B was formed by frames with *t3* values of 15–45°, C with *t3* values of 45–75° and so on till the twelfth cluster L formed. The population of cluster frames shows a Gaussian distribution (Figure 5) with the peak value of 1961 snapshots reached in the middle cluster (G) of the *t3* range between 180° ± 15°.

Pharmacophore development, database screenings, and cytotoxicity assays

On the basis of the above cluster analysis, we focused on the conformations collected in the top-ranked cluster G to build the pharmacophore model. The average structure of the snap-

shots was first generated, which essentially characterized the dynamic behavior of the frames in the cluster. Then, seven features were mapped onto the average structure. They are three H-bond acceptors defined by the nitrogens of pyrazine and the oxygen atom of the ketone, two H-bond donors defined by the hydrazine linker, and the two hydrophobic features were defined by the three-ring fragment of SC161 (Figure 6).

Figure 6. The seven feature model, based on the average structures of the SC161 top-sized cluster, mapping against SC161. Green represents H-bond acceptors; pink represents H-bond donors, and light blue represents hydrophobic features.

The pharmacophore model was applied to screen a subset of our database containing 350,000 small molecules by Catalyst software, and each compound is represented by an ensemble of up to 250 conformations. In total, 938 compounds were mapped by the derived model. With considerations for structural diversity and calculated pharmacokinetic properties, we initially tested 20 compounds and realized that those with oxadiazolopyrazine or quinoline motif showed significant cytotoxicity. We thus extended our search to include more compounds bearing the same scaffolds. Therefore, a total of 35 novel compounds were tested for their cytotoxic properties in a panel of cancer cell lines.

Table 1 lists the compounds identified from this work along with their predicted physiochemical properties and model-fitting values. Cytotoxicity of these compounds against a panel of cancer cell lines are summarized in Table 2. Seventeen compounds showed IC_{50} values <10 μM. Representatives of the oxadiazolopyrazine containing compounds are **2** and **6** with IC_{50} values <3 μM in HCT116 $p53^{+/+}$, HCT116 $p53^{-/-}$, and HEY cells, whereas **15** in the MDA-MB-435 cancer cell and quinoline analogues such as **30** and **32** were, in general, less potent than oxadiazolopyrazines. The best compound, **2**, displayed IC_{50} values <2 μM in HCT116 $p53^{+/+}$, HCT116 $p53^{-/-}$, and HEY cells. Additionally, **2** also exhibited mild toxicity against NIH3T3 ($IC_{50}=8$ μM). Compound **15** exhibited an IC_{50} value of 3.0 μM and 6 ± 1.4 μM against MDA-MB-435 cells and HEY cells, respectively. **19** was toxic to HCT116 $p53^{+/+}$ and $p53^{-/-}$ cells and HEY cells, and yet not toxic to other selected cells at doses up to 10.0 μM. The cytotoxicity of **2** was further confirmed by the colony formation assay. Figure 7 shows a representative result of a colony formation assay in HCT $p53^{+/+}$, and HEY cells treated with **2** at various doses. At a dose of 1 μM of **2**, $>95\%$ colonies were killed in HCT $p53^{+/+}$ cells.

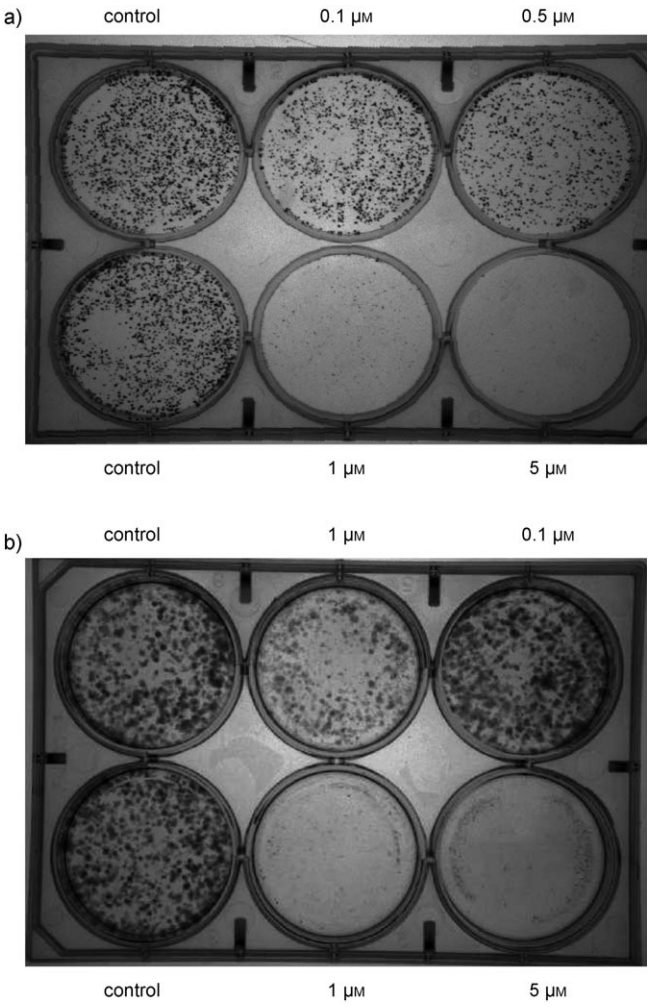

Figure 7. Compound **2** shows significant toxic effect in a) HCT $p53^{+/+}$ and b) HEY cells as observed by colony formation assay of treatment on HCT $p53^{+/+}$ and HEY cancer cells at several doses. At drug concentration $\geq$ 1 μM, more than 95% of colonies were killed in HCT $p53^{+/+}$ cell.

Figure 8 shows the representative compounds **2** and **17** mapped against the pharmacophore model derived from the

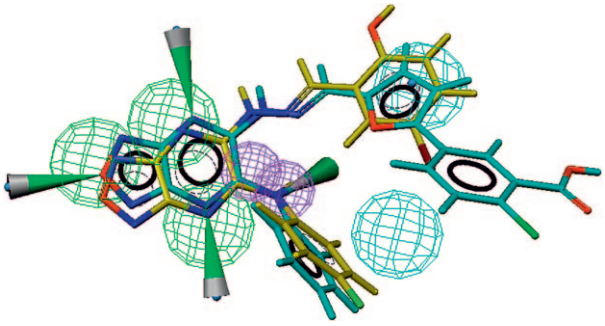

Figure 8. Mapping of selected oxadiazolopyrazines, **2** and **17**, against the pharmacophore model. Green represents H-bond acceptors; pink represents H-bond donors, and light blue represents hydrophobic features. Compounds are displayed as stick models, with carbon atoms in yellow (**2**) and light blue (**17**).

Table 1. Selected physiochemical properties of the tested compounds.[a]

Compd	Structure	MW	pK_a	HBA[b]	HBD[b]	MLog$P$[c]	PSA[d] [Å^2]	Fitting value
1	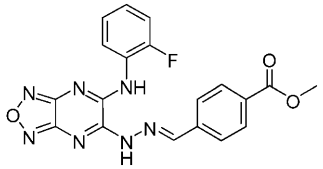	407.4	-	10	2	2.8	133	4.1
2	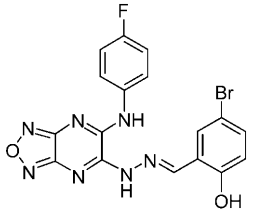	444.2	8.7	9	3	3.1	137	4.3
3	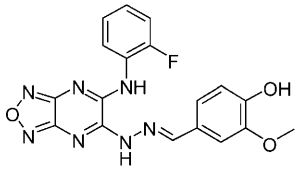	395.4	8.6	10	3	2.2	141	4.1
4	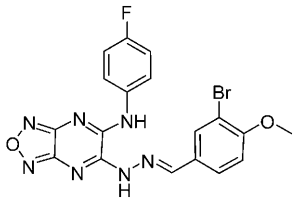	458.3	-	9	2	3.3	107	4.5
5	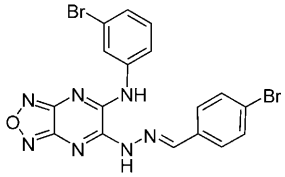	489.1	-	8	2	4.1	105	4.2
6	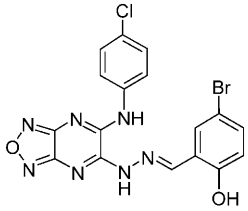	460.7	8.8	9	3	3.2	137	4.3
7	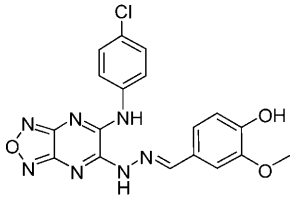	411.8	8.7	10	3	2.4	143	4.6
8	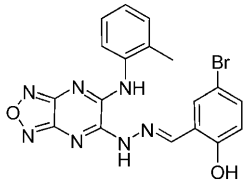	440.3	8.9	9	3	3.2	132	4.2
9	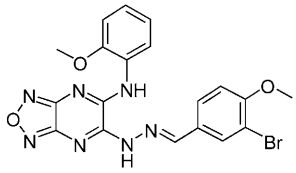	470.3	-	10	2	2.7	106	5.0

Table 1. (Continued)

Compd	Structure	MW	pK_a	HBA[b]	HBD[b]	MLog$P$[c]	PSA[d] [Å^2]	Fitting value
10	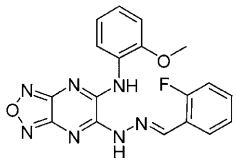	379.3	-	9	2	3.0	105	4.9
11	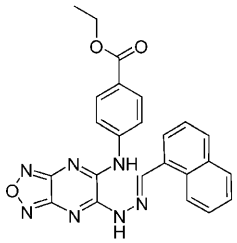	453.5	-	10	2	3.7	136	4.5
12	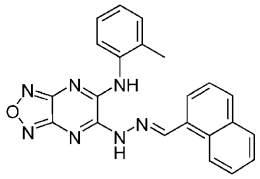	395.4	-	8	2	4.4	101	4.4
13	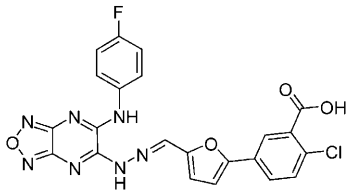	493.8	5.5	11	3	2.8	186	4.3
14	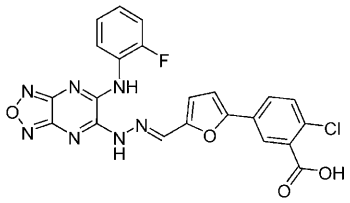	493.8	5.5	11	3	2.8	184	4.2
15	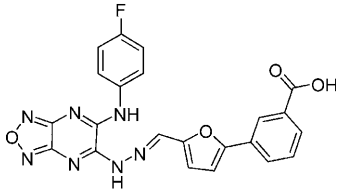	459.4	5.7	11	3	2.6	194	4.3
16	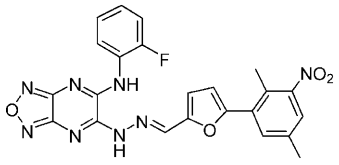	488.4	-	11	2	3.9	170	4.1
17	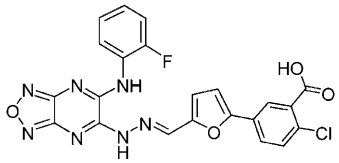	493.8	5.5	11	3	2.8	184	4.2
18	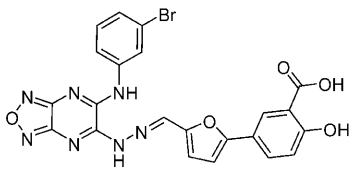	536.3	6.2; 13.6	12	4	2.1	221	4.23

Table 1. (Continued)

Compd	Structure	MW	pK_a	HBA[b]	HBD[b]	MLog$P$[c]	PSA[d] [Å^2]	Fitting value
19	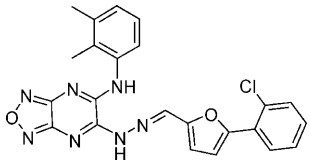	459.9	-	9	2	4.0	97	4.6
20	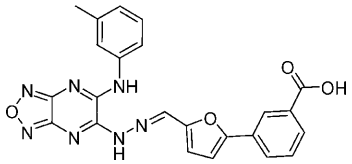	455.4	5.7	11	3	2.7	194	4.2
21	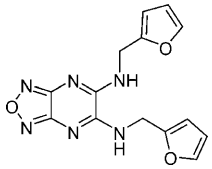	312.3	-	9	2	0.7	130	4.7
22	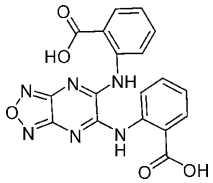	392.3	6.0; 6.2	11	2	-0.9	117	3.5
23	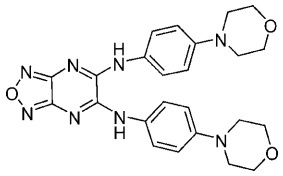	474.5	-	11	2	3.1	137	3.7
24	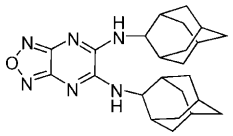	420.6	-	7	2	4.9	101	4.1
25	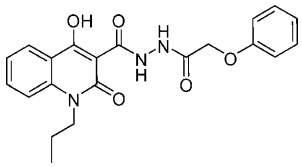	395.4	4.7; 9.6; 10.3	7	3	2.3	129	4.3
26	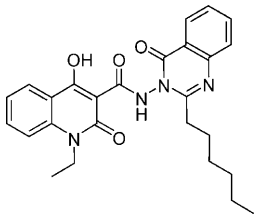	460.5	0.9; 3.4	6	2	3.6	79.3	4.5
27	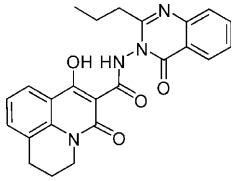	430.5	0.6	6	2	3.2	79	4.0

Table 1. (Continued)

Compd	Structure	MW	pK_a	HBA[b]	HBD[b]	MLog$P$[c]	PSA[d] [Å^2]	Fitting value
28	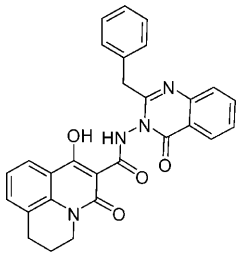	478.5	0.6; 5.1	6	2	3.8	81	3.4
29	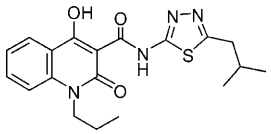	386.5	2.1; 7.8	6	2	2.7	102	4.2
30	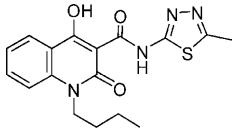	358.4	2.0; 7.7	6	2	2.2	110	4.4
31	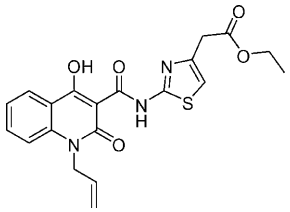	413.4	2.6; 7.9	7	2	1.6	96	4.4
32	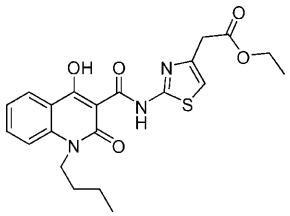	429.5	2.8; 8.1	7	2	1.9	95	4.3
33	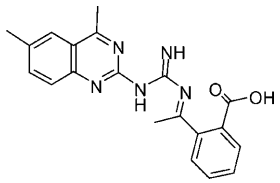	361.4	-0.8; 4.7	7	3	2.9	103	4.2
34	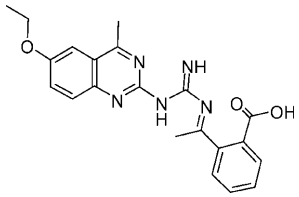	391.4	-0.8; 4.7	8	3	2.6	104	4.4
35	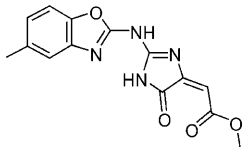	300.3	-3.1	8	2	0.7	114	4.5

[a] All properties were calculated by ADMET Predictor (SimulationsPlus, Inc.), except the fitting values of compound mapping against the pharmacophore model, which were generated by Catalyst (Accelrys, Inc). [b] HBD: the number of H-bond donor atoms; HBA: the number of H-bond acceptor atoms. [c] MLog$P$: Moriguchi octanol–water partition coefficient. [d] PSA: polar solvent accessible surface area [Å^2].

Table 2. Cytotoxicity data of tested compounds in a panel of cell lines.

Cmpd	IC_{50} [μM]				
	HCT116 $p53^{+/+}$	HCT116 $p53^{-/-}$	MDA-MB-435	NIH3T3	HEY
1	>10	10	5	>10	10
2	1.5±1	1.8±0.7	7; 8	6±1.4	1.3±0.4
3	>10	>10	>10	>10	5
4	4	3; 2	10	6	10
5	2	1.1, 1.2	>10	1	2; 3
6	2.7±0.6	1.6±0.7	4±1	2±0.5	1.6±0.6
7	>10	5.5	>10	>10	2
8	2	1.1±0.4	>10	>10	5
9	>20	>10	>20	>10	>10
10	>10	>10	>10	>10	>10
11	>10	2	>10	2	4
12	>10	10	>10	10	>10
13	>10	7	>10	10	>10
14	>10	7	>10	>10	10
15	5; 10	8, 7	3	10	6; 8
16	1.5	0.8±0.1	4	2	0.8
17	7±1	>10	>20	>10	20, 15
18	>10	>10	>10	11	>10
19	3; 2	6; 4	>10	>10	3; 5
20	>10	>10	>10	10	8
21	>20	>10	>20	>10	>20
22	>10	>10	>10	>10	>10
23	>10	>10	>10	>10	>10
24	6; 8	9±1	9	9	8±1.7
25	10	>10	>20	>10	>10
26	>20	>10	>20	20	20
27	>20	>10	>20	12	>20
28	>20	>10	>10	>10	19; 15
29	>20	>10	>20	>10	>20
30	6±3	8	7	5	10; 14
31	20	>10	>10	>10	>10
32	10±1	>10	20	8	15
33	18	5	17; 18	14	5; 3
34	20	10	>20	>10	7
35	5.0	4.2; 3.4	6	11, 6	3.5; 2

Values with standard deviation are from at least three independent experiments and others are as explicitly stated. Each experiment was generated from an average of four independent wells.

structural conformations of cluster G. Because of the multiple conformations of each compound, various mapping orientations against the model were observed. In oxadiazolopyrazines, the three H-bond acceptors could favorably be mapped by the nitrogen atoms, while the N-H could map either of the H-bond donors. On the other hand, only one of the hydrophobic features could be mapped by the aromatic motif.

Conclusions

The purpose of this study was to explore the most probable functional feature orientation in terms of pharmacophore development from a lead compound, SC161, and to identify structurally diverse cytotoxic compounds. Our 10 ns MD studies illustrate the dynamic behavior of SC161 and its preference for a planar conformation. Moreover, the pharmacophore model derived from the ensemble of the most probable conformations was successfully applied to map several compounds showing comparable potency to that of SC161. This study demonstrates that conformational sampling of a small lead molecule is an efficient approach to build a representative pharmacophore model to rationally design cytotoxic agents with different physicochemical and druglike properties.

Experimental and Computational Methods

Molecular dynamics (MD)

The MD studies of SC161 were carried out by GROMACS[13] software package to simulate various biomolecular systems in aqueous or lipid bilayer environments.[14–21] Initially, all the nonpolar hydrogens were removed and only polar hydrogens were kept. The partial charges of SC161, which has polar hydrogens intact, were obtained by ab initio calculation. We applied the unrestricted Hartree–Fock method equipped in the Gaussian program licensed to the High Performance Computer Center (HPCC) of the University of Southern California. The basis set, the set of one-electron wave functions used to build molecular orbital wave functions, was set to STO-3G with spin multiplicity of two. The topology file of SC161 consistent with GROMACS force field was generated by the public access PRODRG online server, and was modified with the partial atomic charges calculated from the above ab initio procedure. Then, SC161 was centered in a box of 414 flexible SPC water molecules, or Simple Point Charge water models, with the size of $2.82\times2.49\times1.86\ nm^3$. GROMACS force field was used to describe bonding and nonbonding interactions. Next, the whole system was gradually equilibrated for 50 ps at each temperature of 50 K, 100 K, 150 K, 200 K, 250 K, and 300 K. Finally, the production phase was simulated for 10 ns at 300 K in the canonical ensemble (NVT, the number of particles N, the volume V, and the temperature T were set to desired values). The chemical bond lengths involving hydrogen atoms were fixed with the SHAKE algorithm.[22] A 2 fs time step was used and both the energy and trajectory output were collected every 2 ps. Van der Waals interactions and short-range electrostatic interactions were truncated at 10.0 Å with the particle mesh Ewald method[23] setting used for long-range electrostatic interactions. Trajectory analysis including cluster analysis were carried out using VEGA software package.[24,25]

Pharmacophore model development and database search

The pharmacophore models were built on the selected snapshots of SC161 conformation, which were taken from the MD trajectory. Initially, the Catalyst software (Accelrys, Inc.) package was used to import the SC161 conformation and map the functional features (H-bond donor, H-bond acceptor, hydrophobic feature, or aromatic ring) onto the frame. To develop the feature model, geometrical constraints were assigned to each feature. For example, co-ordinate and size of the feature, centered at the mapped atom or motif was assigned a radius of 1.3 Å for H-bond donor to avoid feature overlapping, and 1.6 Å for the rest of the features as default. All the selected features were merged into one pharmacophore model. The generated model was used as an independent search query to screen a subset of our 350,000 small-molecule databases. On the basis of intuitive structural classification, we selected compounds representing the diverse chemical and structural space for their cytotoxic properties. In this study, we reported two classes of compounds representing oxadiazolopyrazines and quinolines.

Cytotoxicity Assay

Cell culture: Human breast cancer cells MDA-MB-435 were purchased from the American Type Culture Collection (Manassas, VA). The HCT116 $p53^{+/+}$ and HCT116 $p53^{-/-}$ cells were kindly provided by Dr. Bert Vogelstein (Johns Hopkins Medical Institutions, Baltimore, MD). The human ovarian carcinoma cell line (HEY) which is naturally resistant to cisplatin was kindly provided by Dr. Louis Dubeau, University of Southern California (USC) Norris Cancer Center, and NIH3T3 normal mouse fibroblast cells were kindly provided by Dr. Michael Press from USC Norris Cancer Center. HEY and NIH3T3 cells were maintained as monolayer cultures in RPMI, HCT 116 cells in McCoy's[5]A media and MDA-MB 435 in DMEM. Media were purchased from (Mediatech, Virginia) and supplemented with 10% fetal bovine serum (Gemini-Bioproducts, Woodland, CA), 2 mM L-glutamine, and 5% penicillin/streptomycin from Bio whittaker were purchased from VWR. Cells were incubated at 37 °C in a humidified atmosphere of 5% CO_2. To remove the adherent cells from the flask for passaging and counting, cells were washed with PBS without calcium or magnesium, incubated with a small volume of 0.25% trypsin-EDTA solution (Sigma–Aldrich, St. Louis, MO) for 5–10 min, and washed with culture medium and centrifuged. All experiments were performed using cells at exponential growth stage. Cells were routinely checked for mycoplasma contamination using a PCR-based assay (Stratagene, TX, USA).

Drugs: Stock solutions (10 mM) of all compounds were prepared in DMSO and stored at −20 °C. Further dilutions were made fresh in PBS or cell-culture media immediately before cell treatment.

Cytotoxicity assays: Cytotoxicity was assessed by a 3-(4,5-dimethylthiazol-2-yl)-2,5-diphenyltetrazolium bromide (MTT) assay as previously described.[26] Briefly, cells were seeded in 96-well microtiter plates and allowed to attach overnight. Cells were subsequently treated with continuous exposure to the corresponding drug for 72 h. An MTT solution (at a final concentration of 0.5 mg mL^{-1}) was added to each well, and cells were incubated for 4 h at 37 °C. After removal of the medium, DMSO was added and the absorbance was read at 570 nm. All assays were done in triplicate. The IC_{50} value was then determined for each drug from a plot of log (drug concentration) versus percentage of cells killed.

Colony formation assay: Colony formation assays were also performed to confirm the activity of these compounds as described.[1,27] Briefly, cells were plated in 6-well plates at a density of 500 cells $well^{-1}$ and allowed to attach. The next day, serial dilutions of the corresponding compounds were added and allowed to incubate for 24 h. After exposure, cells were washed in PBS and cultured in drug-free media until colonies were formed (8–10 days). Cells were subsequently washed, fixed with a 1% glutaraldehyde solution for 30 min, and stained with a solution of crystal violet (2%) for 30 min. After staining, cells were thoroughly washed with water. Colonies were imaged on the ChemiDoc Imaging System (Bio-Rad) and counted using the Quantity One quantitation software package (Bio-Rad). The data reported represent means of at least three independent experiments.

Acknowledgements

This work was supported by funds from the Department of Defense OCRP Idea Award, Jeannik M. Littlefield-AACR, and the Wittier Foundation to NN and "Fondazione Carical, Cosenza, Italy" to FG. We are grateful to Dr. Wei Fu associated with Fu Dan University for fruitful discussion particularly on small molecule MD simulations, and to Dr. Laith Q. Al-Mawsawi for careful reading of this manuscript.

Keywords: antitumor agents · cluster analysis · conformational sampling · molecular modeling · molecular dynamics

[1] F. Grande, F. Aiello, O. D. Grazia, A. Brizzi, A. Garofalo, N. Neamati, *Bioorg. Med. Chem.* **2007**, *15*, 288–294.
[2] G. W. Milne, M. C. Nicklaus, S. Wang, *SAR QSAR Environ. Res.* **1998**, *9*, 23–38.
[3] X. Fang, S. Wang, *J. Chem. Inf. Comput. Sci.* **2002**, *42*, 192–198.
[4] O. O. Clement, C. M. Freeman, R. W. Hartmann, V. D. Handratta, T. S. Vasaitis, A. M. Brodie, V. C. Njar, *J. Med. Chem.* **2003**, *46*, 2345–2351.
[5] O. Güner, O. Clement, Y. Kurogi, *Curr. Med. Chem.* **2004**, *11*, 2991–3005.
[6] T. Langer, R. D. Hoffmann, Pharmacophores and pharmacophores searches, in *Methods and Principles in Medicinal Chemistry* (Ed.: G. Folkers), Wiley-VCH, Weinheim, **2006**.
[7] J. Deng, R. Dayam, L. Q. Al-Mawsawi, N. Neamati, *Curr. Pharm. Des.* **2007**, *13*, 129–141.
[8] J. Deng, T. Sanchez, N. Neamati, J. M. Briggs, *J. Med. Chem.* **2006**, *49*, 1684–1692.
[9] R. Dayam, T. Sanchez, N. Neamati, *ChemMedChem* **2006**, *1*, 238–244.
[10] M. O. Taha, Y. Bustanji, A. G. Al-Bakri, A. M. Yousef, W. A. Zalloum, I. M. Al-Masri, N. Atallah, *J. Mol. Graph. Model.* **2007**, *25*, 870–884.
[11] J. Deng, K. W. Lee, T. Sanchez, M. Cui, N. Neamati, J. M. Briggs, *J. Med. Chem.* **2005**, *48*, 1496–1505.
[12] H. A. Carlson, K. M. Masukawa, K. Rubins, F. D. Bushman, W. L. Jorgensen, R. D. Lins, J. M. Briggs, J. A. McCammon, *J. Med. Chem.* **2000**, *43*, 2100–2114.
[13] D. Van Der Spoel, E. Lindahl, B. Hess, G. Groenhof, A. E. Mark, H. J. C. Berendsen, *J. Comput. Chem.* **2005**, *26*, 1701–1718.
[14] W. Fu, J. Shen, X. Luo, W. Zhu, J. Cheng, K. Yu, J. M. Briggs, G. Jin, K. Chen, H. Jiang, *Biophys. J.* **2007**, *93*, 1431–1441.
[15] H. Fan, A. E. Mark, J. Zhu, B. Honig, *Proc. Natl. Acad. Sci. USA* **2005**, *102*, 6760–6764.
[16] A. A. Gurtovenko, I. Vattulainen, *Biophys. J.* **2007**, *92*, 1878–1890.
[17] J. J. James, B. S. Lakshmi, V. Raviprasad, M. J. Ananth, P. Kangueane, P. Gautam, *Protein Eng.* **2003**, *16*, 1017–1024.
[18] A. Palleschi, G. Bocchinfuso, T. Coviello, F. Alhaique, *Carbohydr. Res.* **2005**, *340*, 2154–2162.
[19] W. M. Rockey, A. H. Elcock, *J. Med. Chem.* **2005**, *48*, 4138–4152.
[20] G. R. Stahl, H. D. Höltje, *Pharmazie* **2005**, *60*, 247–253.
[21] H. Verli, J. A. Guimaraes, *Carbohydr. Res.* **2004**, *339*, 281–290.
[22] J.-P. Ryckaert, G. Ciccotti, H. J. C. Berendsen, *J. Comput. Phys.* **1977**, *23*, 327–341.
[23] U. Essmann, L. Perera, M. L. Berkowitz, T. Darden, H. Lee, L. G. Pedersen, *J. Chem. Phys.* **1995**, *103*, 8577–8593.
[24] A. Pedretti, L. Villa, G. Vistoli, *J. Mol. Graphics Modell.* **2002**, *21*, 47–49.
[25] A. Pedretti, L. Villa, G. Vistoli, *J. Cold Reg. Eng. J. Comput. Aided Mol. Des.* **2004**, *18*, 167–173.
[26] J. Carmichael, W. G. DeGraff, A. F. Gazdar, J. D. Minna, J. B. Mitchell, *Cancer Res.* **1987**, *47*, 936–942.
[27] A. Munshi, M. Hobbs, R. E. Meyn, *Methods Mol. Med.* **2005**, *110*, 21–28.

Received: July 10, 2008
Revised: September 2, 2008
Published online on November 4, 2008

